Atomically Thin Al$_{2}$O$_{3}$ Films for Tunnel Junctions

Jamie Wilt, Youpin Gong, Ming Gong, Feifan Su, Huikai Xu, Ridwan Sakidja, Alan Elliot,

Rongtao Lu, Shiping Zhao, Siyuan Han, and Judy Z. Wu

Atomically-Thin Al$_2$O$_3$ Films for Tunnel Junctions

Jamie Wilt[1*], Youpin Gong[1], Ming Gong[1], Feifan Su[2], Huikai Xu[2], Ridwan Sakidja[3],

Alan Elliot[1], Rongtao Lu[1], Shiping Zhao[2], Siyuan Han[1] and Judy Z. Wu[1*]

[1]*Department of Physics and Astronomy, University of Kansas, Lawrence, Kansas, 66045, USA*

[2]*Institute of Physics, Chinese Academy of Science, Beijing, China 100190*

[3]*Department of Physics, Astronomy and Materials Science, Missouri State University,*

Springfield, MO 65897, USA.

Metal-Insulator-Metal tunnel junctions (MIMTJ) are common throughout the microelectronics industry. The industry standard AlO$_x$ tunnel barrier, formed through oxygen diffusion into an Al wetting layer, is plagued by internal defects and pinholes which prevent the realization of atomically-thin barriers demanded for enhanced quantum coherence. In this work, we employed *in situ* scanning tunneling spectroscopy along with molecular dynamics simulations to understand and control the growth of atomically thin Al$_2$O$_3$ tunnel barriers using atomic layer deposition (ALD). We found that a carefully tuned initial H$_2$O pulse hydroxylated the Al surface and enabled the creation of an atomically-thin Al$_2$O$_3$ tunnel barrier with a high quality M-I interface and a significantly enhanced barrier height compared to thermal AlO$_x$. These properties, corroborated by fabricated Josephson Junctions, show that ALD Al$_2$O$_3$ is a dense, leak-free tunnel barrier with a low defect density which can be a key component for the next-generation of MIMTJs.

I. INTRODUCTION

Metal-insulator-metal tunnel junctions (MIMTJs) are fundamental building blocks for microelectronics including magnetic tunnel junctions for spintronics and fast access nonvolatile magnetic memory, and Josephson Junctions (JJs) for particle detectors, magnetic field sensors, and qubits for quantum computation. The performance of MIMTJs depends critically on the quality of the insulating tunnel barrier [1]. Considering native oxides can naturally form on the surface of most metals, producing an atomically-thin, uniform, and pinhole-free tunnel barrier represents a major challenge in the research of MIMTJs. In $Nb/Al/AlO_x/Nb$ JJs for example, an ultrathin (< 1 nm) tunnel barrier is the key to preserve phase coherence across the superconducting Nb electrodes, since the critical current (I_c) through the JJ exponentially decays with the barrier thickness [2]. Thermal oxidation has been the industry standard to produce AlO_x tunnel barriers for JJs through *in situ* oxygen diffusion into an Al wetting layer (Fig. 1(a)) [3]. However this diffusion mediated process has difficulty achieving a uniform tunnel barrier with a well-defined thickness [4]. Despite successful commercial applications of these JJs in devices such as superconducting quantum interference devices and voltage standards, two-level defects (TLDs) in the AlO_x tunnel barrier are one of the major sources of decoherence in superconducting qubits [5].

Atomic Layer Deposition (ALD) is a promising alternative for the synthesis of atomically-thin tunnel barriers for high performance MIMTJs. ALD is a chemical vapor process that utilizes self-limited surface reactions to grow films one atomic layer at a time (Fig. 1(b)). Specifically, ALD Al_2O_3 consists of a series of alternating precursor pulses of H_2O and trimethylaluminum which react at the sample's surface [6]. This process results in a fully oxidized, uniform and pinhole-free Al_2O_3 film with atomic-scale thickness control. In addition,

it's reduced bulk loss tangent implies that JJs with ALD Al_2O_3 tunnel barriers may have a significantly reduced TLD density [7].

However, precise ALD growth and nucleation on metals remains challenging. The MIMTJ electrode and tunnel barrier deposition must be carried out *in situ* without breaking vacuum to avoid native oxides. ALD nucleation on inert metal surfaces, such as Pt and Au, can be completely frustrated for the first 30-50 cycles of alternating precursor pulses whereas for reactive metals, such as Al, even *in situ* deposited films can acquire an interfacial layer (IL) of AlO_x up to ~2 nm thick [8-10]. In a previous work, fabricated $Nb/Al/Al_2O_3/Nb$ JJs using *in situ* ALD of Al_2O_3 had an IL >0.5 nm in thickness which was attributed to poor vacuum pressure (~500 mTorr) during sample transfer and pre-ALD sample heating [9,11,12]. This IL prevented the realization of truly atomically-thin tunnel barriers and led to poor quality JJs. Herein, we resolve these challenges by performing the sample transfer and pre-ALD heating under high-vacuum (HV) and report the first successful fabrication of atomically-thin ALD Al_2O_3 tunnel barriers. *In situ* scanning tunneling spectroscopy (STS) was employed to probe the growth mechanisms and physical properties of the ALD Al_2O_3 tunnel barriers and JJs were fabricated to illustrate the viability of ALD Al_2O_3 tunnel barriers for MIMTJs.

II. EXPERIMENTAL

For samples which underwent *in situ* STS characterization, a bilayer of Nb (20 nm)/Al (7 nm) was magnetron sputtered onto a Si/Au(50 nm) substrate which was mechanically clamped to the sample stage to serve as the ground contact for the Scanning Tunneling Microscope (STM) from RHK Technology. The Au was thermally evaporated onto an updoped Si wafer with a native oxide. An *ex situ* Atomic force microscope measured it's surface roughness to be ~1.2

nm. Immediately following the Al sputtering, an aluminum oxide tunnel barrier was formed by either thermal oxidation or ALD. For the thermal oxidation samples, Ultra high Purity 99.993% O_2 was introduced to the sputtering chamber for an oxygen exposure of 1150, 1020, and 42 torr-seconds, respectively. The samples with ALD tunnel barriers were transferred to a preheated ALD chamber and then heated for 75 min or 15 min to a temperature of 200 °C - 220 °C. Following sample heating, reagents H_2O and trimethylaluminum were pulsed into the ALD chamber for 1-3 s with a purge step between pulses to deposit the ALD Al_2O_3 tunnel barriers.

After tunnel barrier fabrication, the samples were transferred under HV, *in situ*, to the STM chamber which had a pressure of $\sim 2 \times 10^{-10}$ Torr. A single mechanically-cleaved Pt-Ir STM tip was used for all STS studies. Constant height IV and *dI/dV* spectroscopy were taken simultaneously using the lock-in amplifier method with a voltage modulation of 100 mV at 1 kHz. The tunnel barrier height was estimated by the intersection of two bisquare-method linear fits to ln(*dI/dV*) similar to the method reported in [13]. The endpoints for this linear fits were determined by eye. One line fit the band gap regime, and the other the conduction band. This ln(*dI/dV*) linear fit method was chosen over IV or *(dI/dV)/(I/V)* fit methods for it's insensitivity to high noise in STS spectra [14,15]. Approximately 40-80 *dI/dV* spectra were taken on each sample >100 nm apart from one another in order to get reasonable statistics on the sample's surface.

The *Ab-initio* molecular dynamics simulations for the initial water activation pulse used a 2x2 supercell of face-centered cubic Al (111) under constant equilibrium volume and temperature and adopted Bohn-Oppenheimer molecular dynamics as implemented in VASP [16-18]. The canonical ensemble simulations employed the London dispersion correction using the vdW-DF functional of Langreth and Lundqvist [19] with a high plane wave energy cut-off of

450 eV to ensure high precision. The electronic and ionic convergence criteria used were 10^{-4} eV and 10^{-3} eV respectively. Energy barrier and reaction pathways were investigated using the Climbing-Image-Nudge Elastic Band method [20] as implemented in the Quantum Espresso code [21].

Nb-Al/ALD-Al$_2$O$_3$/Nb trilayers were fabricated in a homemade deposition system, which integrated Ultra-high Vacuum (UHV) sputtering and ALD *in situ* [11,22]. For comparison, traditional thermally oxidized Nb-Al/AlO$_x$/Nb trilayers were also fabricated. The Nb films were sputtered at 1.7 nm/s to minimize the formation of NbO$_x$ from trace oxygen. The sputtering chamber had a base pressure of ~10^{-7} Torr or better and the sample stage was chilled-water cooled to approximately 10 °C. The bottom Nb was 150 nm, and the top Nb was 50 nm. Samples with ALD tunnel barriers were transferred *in situ* to the preheated ALD chamber, and heated for 75 min under HV. The wafer design used to investigate the quality of tunnel barriers contained 12 square junctions of four different sizes ranging from 4 μm ×4 μm to 10 μm ×10 μm and was fabricated using the self-aligned niobium trilayer process described in [23]. The JJ's dc current-voltage characteristics (IVC) were measured at 4.2 K in a liquid helium storage dewar.

III. RESULTS AND DISCUSSION

A. *In situ* Scanning Tunneling Spectroscopy and molecular dynamics simulations

ALD is a low-vacuum process that is incompatible with UHV required for both physical vapor deposition of functional electrodes and *in situ* characterization using STM. To address this issue, an integrated Sputtering-ALD-STM system was developed to allow for UHV deposition of metals, UHV STM characterization of surfaces and interfaces, and HV (10^{-6}-10^{-7} Torr) *in situ* sample transportation between the chambers [22]. This HV transport minimizes the metal

electrode's exposure to trace gases and hence IL formation. An additional challenge to avoid IL formation is the sample heating time required to bridge the temperature difference between sputtering at 10-14 ℃ and ALD at 200 °C - 220 °C. To address this challenge, the samples were inserted into a preheated ALD chamber for different times and dynamically heated to 200 °C - 220 °C under HV. Specifically, two dynamic heating times of 75 min and 15 min are presented in this work to illustrate the importance of controlling this procedure in order to achieve a clean interface between the Al and ALD Al_2O_3 tunnel barrier.

In Fig. 2(a), STS *dI/dV* spectra were taken *in situ* at room temperature on Nb/Al bilayer structures which were exposed to these two dynamic heating times. The spectrum for the 75 min heated sample (Fig. 2(a)-I) resembles that of a highly defective tunnel barrier. In fact, it has characteristics similar to the thermal AlO_x tunnel barrier (discussed later in Fig. 3) [24,25]. In contrast, the spectrum for the 15 min heated sample (Fig. 2(a)-II) closely matches the conductive spectrum measured from a calibration sample that was directly transferred to the STM chamber after Al sputtering without going through any heating (Fig. 2(a)-II, insert). These spectra suggest that HV and short exposure between Physical Vapor Deposition and ALD are critical to minimize IL formation.

To initiate the ALD Al_2O_3, the Al wetting layer was exposed to a H_2O pulse to hydroxylate its surface. In order to understand the kinetics of this hydroxylation process, the behavior of H_2O on the Al surface was investigated using *Ab-initio* molecular dynamics and Climbing-Image-Nudge Elastic Band simulations. When only one H_2O molecule (i.e. without H_2O molecules in proximity) is present on the Al surface, H_2O dissociation into OH^- is thermodynamically unfavorable, as shown in Fig. 2(b)-I, II. However, when multiple H_2O molecules are present on the Al (111) surface, dissociation occurs after just a few ps (Fig. 2(b)-

III, IV). A proton transfer between nearby H_2O molecules creates OH^- and H_3O^+, followed by H_3O^+ dissociation into H_2O_{ad} and H^+_{ad}. We found this reaction to be net **exothermic** with a ~0.5 eV energy barrier (See the Supplementary Material [26]). These simulations suggest that the H_2O areal density from the H_2O pulse is crucial to facilitate an efficient hydroxylation reaction which will form a uniform monolayer of OH^- on the Al surface. The stability of these OH^- groups is also critical as dissociation into O and H^+_{ads} could lead to oxygen diffusion into the Al wetting layer and IL formation. Fortunately, these OH^- groups do not readily dissociate at typical ALD temperatures of ~200 ºC. However, this dissociation may become a concern at significantly higher temperatures as the shown in our simulations [27].

In order to experimentally probe this hydroxylation process, one cycle of ALD Al_2O_3 was performed on an Al wetting layer with an initial H_2O pulse of variable duration. Figure 2(a)-III depicts a representative *dI/dV* spectrum for a 1-cycle ALD Al_2O_3 tunnel barrier with an initial H_2O pulse of 2 s in duration. The Figure 2(a)-III insert shows the corresponding IV curve. This *dI/dV* spectrum displays a well-defined tunnel barrier with a barrier height, E_b, of ~1.56 eV and indicates that an atomically-thin tunnel barrier (Fig. 2(a)-III, schematic) can be obtained using this UHV Physical Vapor Deposition-ALD approach on a clean Al wetting layer (Fig. 2(a)-II, schematic) through careful control of the ALD growth in order to minimize IL formation (Figure 2(a)-I, schematic).

Figure 2(c) reveals the one-cycle ALD Al_2O_3 coverage on the Al wetting layer as the initial H_2O pulse duration was varied from 1-3 s. The ALD Al_2O_3 coverage was defined as the percentage of STS spectra, taken from random locations on the sample, which showed a sharp conduction band onset and an E_b consistent with ALD samples of higher cycle number (see Fig. 3). The ALD Al_2O_3 surface coverage increased from ~54% at 1 s pulse duration to ~93% at 2 s

duration. These experimentally observed time frames suggest that long initial H_2O pulses, on the order of seconds, are required for H_2O molecules, adsorbed to the Al surface, to reach a high enough areal molecular density for an efficient dissociation into OH^- to occur. Interestingly, longer H_2O pulses were found to be detrimental to the ALD Al_2O_3 surface coverage. The remaining, non-ALD, spectra on the Al surface were either conductive or had very high noise and were unstable under the STM electric field. While the nature of these non-ALD, non-conductive spectra remains to be a topic of further investigation, we speculate that very long H_2O pulses may lead to H_2O clusters instead of monolayer formation on the Al surface. These clusters may slow down or prohibit uniform surface hydroxylation.

In addition to its paramount role in nucleation, the hydroxylation of the Al wetting layer prevents oxygen from diffusing into the Al to form an IL during the ALD process. This argument is supported by the dI/dV characteristics and E_b observed for the thermal AlO_x and the ALD Al_2O_3 tunnel barriers. The dI/dV spectra for a thermal AlO_x tunnel barrier of ~1.3 nm, in estimated thickness [12], is shown alongside a 10-cycle ALD Al_2O_3 tunnel barrier with a comparable thickness of ~1.2 nm in Fig. 3(a). The ALD Al_2O_3 spectrum has a significantly sharper conduction band onset than the thermal AlO_x spectrum, suggesting that the ALD Al_2O_3 tunnel barrier has a much more ordered and less-defective internal structure [24,25,28,29]. This improved internal structure is corroborated by the higher ALD Al_2O_3 E_b shown in Fig. 3(b). Specifically, E_b values of ~1.00 eV and ~1.42 eV were observed for the ALD Al_2O_3 tunnel barriers with 75 min heating and 15 min heating respectively whereas the thermal AlO_x counterpart was just ~0.67 eV. Other groups have reported similar thermal AlO_x E_b values [12,30]. In addition, the ALD Al_2O_3 samples with 15 min of heating had a band gap of ~2.5 eV. This high band gap is remarkable because it is comparable to the ultrathin (~1.3 nm) epitaxial

Al$_2$O$_3$ band gap [31]. The ALD Al$_2$O$_3$ tunnel barrier also displayed a hard-breakdown type behavior under the STM electric field which is typical for epitaxial Al$_2$O$_3$ thin films [32]. In great contrast, the thermal AlO$_x$ tunnel barriers broke-down in a soft-breakdown manner due to defect migration within the barrier [24,25,32-35]. We should note that the 75 min heated samples displayed both types of breakdown, which is consistent with the thin IL found in Fig. 2(a). However the absence of soft-breakdown in the ALD Al$_2$O$_3$ tunnel barrier with 15 min heating can be taken as an indicator that no significant IL is present on its metal-insulator interface.

It is also particularly interesting that the ALD Al$_2$O$_3$ E_b value was maintained as the number of ALD cycles, N, varied from 1 to 10 (Fig. 3(b)). This trend is particularly demonstrated in the ALD Al$_2$O$_3$ samples with 15 min heating (blue) and further indicates that a significant metal-insulator IL is not present-as an IL would have disproportionately affected the samples with smaller N's by lowering their E_b values. For the ALD Al$_2$O$_3$ samples with 75 min heating (black), an IL was confirmed by the slight E_b reduction of 0.11 eV as N was reduced to 1 and 2 from larger values. An additional effect of this IL is demonstrated by the E_b improvement as the sample heating time was reduced from 75 min (black line) to 15 min (blue line). Nevertheless, this overall ALD Al$_2$O$_3$ E_b consistency with thickness is remarkable because it illustrates that the ALD process can produce high quality Al$_2$O$_3$ down to the atomically-thin limit. In contrast, the thermal AlO$_x$ E_b has a significant thickness dependence in the lower nominal thickness range, although a value of 0.67 eV is maintained at 0.6-1.3 nm thickness. This E_b thickness dependence is reflected by the dramatic increase in critical current density, J_c, observed in JJs with thermal AlO$_x$ tunnel barriers as the oxygen exposure drops below ~10^3 Pa-s,

or ~0.4 nm in thickness [2,12]. Furthermore, a complete tunnel barrier is not even formed in this regime as the tunneling current is dominated by pinholes.

B. Josephson Junction characterization

To demonstrate how this ALD Al_2O_3 tunnel barrier performs in a demanding MIMTJ application, JJs were fabricated and their IVCs measured at 4.2 K. The IVC of a 5-cycle junction with a designed area of 10 µm x 10 µm is shown in Fig. 4(a). This IVC has a low subgap leakage current and is highly nonlinear-as expected for Superconductor-Insulator-Superconductor tunnel junctions. The small current step at $V = \Delta/e$ of the IVC is most likely caused by Andreev reflection at the interface between the bottom Nb electrode and the 7-nm Al wetting layer of the Nb-Al-Al_2O_3-Nb structure [36] and not due to transport through pinholes-as discussed in [37]. The superconducting gap voltage was $V_g \equiv 2\Delta/e \cong 2.6$ mV and did not depend on N. In addition, the IR_n versus voltage V, where R_n is taken to be the dynamic resistance at 5 mV, is nearly identical for JJs with different N; indicating good reproducibility in our junction fabrication process. These JJs are of considerably higher quality than ALD Al_2O_3 JJs fabricated in our previous work which had a dramatic critical current, I_c, suppression due to charge scatter sites in the metal-insulator IL [11].

Recently, by measuring the dependence of the JJ's critical current density on oxygen exposure, a proxy for tunnel barrier thickness d, the thermal AlO_x tunnel barrier E_b was found to be ~0.64 eV [12,38]. Notice that it is very difficult to calibrate the relationship between thickness, d, and oxygen exposure. In contrast, due to the self-limited, layer-by-layer growth

nature of ALD, the growth rate of the ALD Al_2O_3 tunnel barrier has been precisely calibrated as $d_{ALD} = 0.115 \pm 0.005$ nm/cycle [9]. To determine the ALD JJ E_b, the measured critical current density, $G_n = (R_nA)^{-1} \propto J_c$, was plotted against d_{ALD} in Fig. 4(b). Because thermal and magnetic field fluctuations have a strong effect on the switching current but have essentially no effect on the normal-state resistance, R_n, especially for JJs with small critical currents, it is much more reliable to extract E_b by fitting the exponential dependence of G_n versus d_{ALD}.

$$G_n = G_0 \exp\left(-\frac{\sqrt{2m_eE_b}}{h} d_{ALD}\right), \qquad (1)$$

where m_e is the electron mass, $\hbar$ is the Planck constant, and G_0 is the specific conductance for $d_{ALD} = 0$. The tunnel barrier height determined from the best fit was $E_b = 1.10 \pm 0.06$ eV. This E_b value agrees well with our STS measurements.

Ideal tunnel junctions require a uniform tunnel barrier with no microscopic pinholes. Pinholes lead to subgap leakage current and a distorted magnetic field dependence on I_c. The magnetic field dependence of the critical current, $I_c(H)$, for a 5-cycle junction is shown in Fig. 4(c). Complete I_c suppression at the first minimum and a symmetric shape was observed. The applied magnetic field H was in the plane of the junction (x-y plane) and parallel to the vertical edges of the 7 μm x 7 μm junction (although a small misalignment cannot be ruled out). This symmetric behavior is consistent with a uniform insulating tunnel barrier with negligible leakage current and pinholes [39].

A denser tunnel barrier should have fewer atomic-scale TLDs. TLDs have been identified as one of the major sources of decoherence for superconducting qubits, which are

considered one of the strongest candidates for the implementation of scalable quantum computing [40]. It has been observed that TLDs embedded inside the oxide tunnel barrier and/or at the superconductor/oxide interface can couple strongly to Josephson qubits. These TLDs lead to splitting in the transition energy spectrum of the qubit, large fluctuations in I_c, and distortions in junction's switching current distribution $P_{sw}(I)$ [41-43]. Therefore, $P_{sw}(I)$ can be used as a diagnostic tool for the detection of TLDs in tunnel barriers which couple strongly to the junction. Figure 4(d) shows the experimental $P_{sw}(I)$ which was obtained using the conventional time-of-flight technique [44-46] with a constant current sweeping rate of 5 mA/s in a very well filtered and shielded cryostat suitable for coherent quantum dynamics of Josephson qubits [46,47]. In order to reduce the effect of self-heating, a 7 μm x 7 μm, 10-ALD cycle junction with a very low critical current density of $J_c = 9.7$ A/cm^2 was selected for the $P_{sw}(I)$ measurements. The critical current of the junction, $I_c = 4.757 \pm 0.003$ μA, was determined by fitting the measured $P_{sw}(I)$ to the prediction from thermal activation theory with the critical current as the adjustable parameter [44-46]. The junction's shunt capacitance was estimated to be, C ≈ 2.2 pF, from the 45 fF/μm^2 specific capacitance of low-J_c Nb JJs and the junction's nominal area [48]. Typical $P_{sw}(I)$ curves obtained at $T = 0.76$ K and 1.17 K are shown in Fig. 4(d). The measured distributions agree very well with those calculated from thermal activation theory. The absence of anomalies in the $P_{sw}(I)$ distributions is consistent with a lack of TLDs which couple strongly to the junction in the tunnel barrier and/or at the superconductor-insulator interface.

IV. SUMMARY AND CONCLUSIONS

In summary, an *in situ* STS study has been carried out to understand the nucleation mechanisms of ALD Al$_2$O$_3$ on an Al wetting layer. We have found that a well-controlled

hydroxylation of the Al wetting layer, through a carefully controlled first H_2O pulse, is the key to enable the creation of an atomically-thin ALD Al_2O_3 tunnel barrier which is of significantly higher quality than the industrial standard thermal AlO_x tunnel barrier. Specifically, the ALD Al_2O_3 tunnel barrier has a high E_b of 1.42 eV which is maintained as the barrier thickness is varied in the range of 0.12-1.2 nm. Furthermore, this ALD Al_2O_3 tunnel barrier has a band gap of ~2.5 eV and exhibits hard electrical breakdown behavior similar to high-quality epitaxial Al_2O_3 thin films. In contrast, the thermal AlO_x tunnel barrier has a low E_b of ~0.67 eV only in the barrier thickness range exceeding 0.6 nm. At smaller thicknesses, enhanced soft electrical breakdown occurs and the E_b decreases. Finally, the pre-ALD exposure of the Al surface in the ALD chamber, even in high vacuum, was found to be critical and must be minimized to prevent AlOx IL formation which leads to a reduced E_b, especially at smaller barrier thicknesses. This result demonstrates for the first time, to our knowledge, the viability of the ALD process to create an atomically-thin Al_2O_3 tunnel barrier which has a significantly denser, less defective internal structure than thermal AlO_x-as demanded for the next generation of high performance MIMTJs.

ACKNOWLEDGEMENTS

Author Contributions

J.S.W., J.Z.W. and S.Y.H. designed the experiment. J.S.W. prepared the samples for STS and A.E. prepared JJs with the assistance of Melisa Xin. J.S.W. performed STS characterization and Y.P.G., A.E. M.G., F.F.S., H.K.X., R.T.L. carried out JJ characterization. R.S. did the simulations. All authors contributed to discussions of the results. J.S.W, S.Y.H., S.P.Z., R.S., and J.Z.W. led the effort in development of the manuscript.

References

[1]   L. A. Abelson and G. L. Kerber, Superconductor integrated circuit fabrication technology, Proceedings of the IEEE 92, 1517 (2004).

[2]   A. W. Kleinsasser, R. E. Miller, and W. H. Mallison, Dependence of critical current density on oxygen exposure in Nb-AlO/sub x/-Nb tunnel junctions, Applied Superconductivity, IEEE Transactions on 5, 26 (1995).

[3]   M. Gurvitch, M. Washington, and H. Huggins, High quality refractory Josephson tunnel junctions utilizing thin aluminum layers, Applied Physics Letters 42, 472 (1983).

[4]   B. Seeber, *Handbook of applied superconductivity* (CRC press, 1998), Vol. 2.

[5]   R. McDermott, Materials origins of decoherence in superconducting qubits, Applied Superconductivity, IEEE Transactions on 19, 2 (2009).

[6]   S. M. George, Atomic Layer Deposition: An Overview, Chemical Reviews 110, 111 (2009).

[7]   M. Khalil, M. Stoutimore, S. Gladchenko, A. Holder, C. Musgrave, A. Kozen, G. Rubloff, Y. Liu, R. Gordon, and J. Yum, Evidence for hydrogen two-level systems in atomic layer deposition oxides, Applied Physics Letters 103, 162601 (2013).

[8]   M. Groner, J. Elam, F. Fabreguette, and S. M. George, Electrical characterization of thin Al_2O_3 films grown by atomic layer deposition on silicon and various metal substrates, Thin Solid Films 413, 186 (2002).

[9]   A. J. Elliot, G. Malek, L. Wille, R. Lu, S. Han, J. Z. Wu, J. Talvacchio, and R. M. Lewis, Probing the Nucleation of in Atomic Layer Deposition on Aluminum for Ultrathin Tunneling Barriers in Josephson Junctions, Applied Superconductivity, IEEE Transactions on 23, 1101405 (2013).

[10]   K. Kukli, M. Ritala, T. Pilvi, T. Aaltonen, J. Aarik, M. Lautala, and M. Leskelä, Atomic layer deposition rate, phase composition and performance of HfO_2 films on noble metal and alkoxylated silicon substrates, Materials Science and Engineering B 118, 112 (2005).

[11]   R. Lu, A. J. Elliot, L. Wille, B. Mao, S. Han, J. Z. Wu, J. Talvacchio, H. M. Schulze, R. M. Lewis, and D. J. Ewing, Fabrication of Josephson Junctions Using In Situ Magnetron Sputtering and Atomic Layer Deposition, Applied Superconductivity, IEEE Transactions on 23, 1100705 (2013).

[12]   X. Kang, L. Ying, H. Wang, G. Zhang, W. Peng, X. Kong, X. Xie, and Z. Wang, Measurements of tunneling barrier thicknesses for Nb/Al–AlOx/Nb tunnel junctions, Physica C: Superconductivity 503, 29 (2014).

[13]   M. M. Ugeda, A. J. Bradley, S.-F. Shi, H. Felipe, Y. Zhang, D. Y. Qiu, W. Ruan, S.-K. Mo, Z. Hussain, and Z.-X. Shen, Giant bandgap renormalization and excitonic effects in a monolayer transition metal dichalcogenide semiconductor, Nature materials 13, 1091 (2014).

[14]   R. M. Feenstra, S. Gaan, G. Meyer, and K. Rieder, Low-temperature tunneling spectroscopy of Ge (111) c (2× 8) surfaces, Physical Review B 71, 125316 (2005).

[15]   L. Dorneles, D. Schaefer, M. Carara, and L. Schelp, The use of Simmons' equation to quantify the insulating barrier parameters in Al/AlO x/Al tunnel junctions, Applied physics letters 82, 2832 (2003).

[16]   G. Kresse and J. Hafner, *Ab initio* molecular-dynamics simulation of the liquid-metal–amorphous-semiconductor transition in germanium, Physical Review B 49, 14251 (1994).

[17]   G. Kresse and J. Hafner, *Ab-initio* molecular dynamics for liquid metals, Physical Review B 47, 558 (1993).

[18]   J. Hafner, Ab-initio simulations of materials using VASP: Density-functional theory and beyond, Journal of Computational Chemistry 29, 2044 (2008).

[19] M. Dion, H. Rydberg, E. Schröder, D. C. Langreth, and B. I. Lundqvist, Van der Waals Density Functional for General Geometries, Physical Review Letters 92, 246401 (2004).

[20] D. Sheppard, R. Terrell, and G. Henkelman, Optimization methods for finding minimum energy paths, The Journal of Chemical Physics 128, 134106 (2008).

[21] G. Paolo, B. Stefano, B. Nicola, C. Matteo, C. Roberto, C. Carlo, C. Davide, L. C. Guido, C. Matteo, D. Ismaila, C. Andrea Dal, G. Stefano de, F. Stefano, F. Guido, G. Ralph, G. Uwe, G. Christos, K. Anton, L. Michele, M.-S. Layla, M. Nicola, M. Francesco, M. Riccardo, P. Stefano, P. Alfredo, P. Lorenzo, S. Carlo, S. Sandro, S. Gabriele, P. S. Ari, S. Alexander, U. Paolo, and M. W. Renata, QUANTUM ESPRESSO: a modular and open-source software project for quantum simulations of materials, Journal of Physics: Condensed Matter 21, 395502 (2009).

[22] A. J. Elliot, G. A. Malek, R. Lu, S. Han, H. Yu, S. Zhao, and J. Z. Wu, Integrating atomic layer deposition and ultra-high vacuum physical vapor deposition for in situ fabrication of tunnel junctions, Review of Scientific Instruments 85, 073904 (2014).

[23] W. Chen, V. Patel, and J. E. Lukens, Fabrication of high-quality Josephson junctions for quantum computation using a self-aligned process, Microelectronic Engineering 73, 767 (2004).

[24] E. Tan, P. Mather, A. Perrella, J. Read, and R. Buhrman, Oxygen stoichiometry and instability in aluminum oxide tunnel barrier layers, Physical Review B 71, 161401 (2005).

[25] P. Mather, A. Perrella, E. Tan, J. Read, and R. Buhrman, Tunneling spectroscopy studies of treated aluminum oxide tunnel barrier layers, Applied Physics Letters 86, 242504 (2005).

[26] See Supplementary Material at [URL] for the reaction pathway of this dehydrogenation process which incluces Refs [20,21].

[27] See Supplementary Material at [URL] for more details on the temperature dependence of this protonation reaction which includes Refs [20,21].

[28] J. M. Martinis, Superconducting phase qubits, Quantum Information Processing 8, 81 (2009).

[29] X. J. Kang, L. L. Ying, H. Wang, G. F. Zhang, W. Peng, X. Y. Kong, X. M. Xie, and Z. Wang, Measurements of tunneling barrier thicknesses for Nb/Al-AlOx/Nb tunnel junctions, Physica C 503, 29 (2014).

[30] J.-G. J. Zhu and C. Park, Magnetic tunnel junctions, Materials Today 9, 36 (2006).

[31] C. Dietrich, H.-G. Boyen, and B. Koslowski, Characterization of ultrathin insulating Al2O3 films grown on Nb (110)/sapphire (0001) by tunneling spectroscopy and microscopy, Journal of applied physics 94, 1478 (2003).

[32] N. Magtoto, C. Niu, B. Ekstrom, S. Addepalli, and J. Kelber, Dielectric breakdown of ultrathin aluminum oxide films induced by scanning tunneling microscopy, Appl Phys Lett 77, 2228 (2000).

[33] W. Rippard, A. Perrella, F. Albert, and R. Buhrman, Ultrathin aluminum oxide tunnel barriers, Physical review letters 88, 046805 (2002).

[34] A. Perrella, W. Rippard, P. Mather, M. Plisch, and R. Buhrman, Scanning tunneling spectroscopy and ballistic electron emission microscopy studies of aluminum-oxide surfaces, Physical Review B 65, 201403 (2002).

[35] P. Mather, Cornell University, 2006.

[36] V. Shaternik, A. Shapovalov, M. Belogolovskii, S. Döring, S. Schmidt, and P. Seidel, Tunneling characteristics of superconducting junctions with inhomogeneous tunnel barriers, Materialwissenschaft und Werkstofftechnik 44, 205 (2013).

[37] T. Klapwijk, G. Blonder, and M. Tinkham, Explanation of subharmonic energy gap structure in superconducting contacts, Physica B+ C 109, 1657 (1982).

[38] There was a factor of 2 error in the exponent of Eq (1) of Ref. [12]. Once corrected, their thermal AlOx Eb was 0.64 eV.

[39] R. Dynes and T. Fulton, Supercurrent density distribution in Josephson junctions, Physical Review B 3, 3015 (1971).

[40] L.-C. Ku and C. Y. Clare, Decoherence of a Josephson qubit due to coupling to two-level systems, Physical Review B 72, 024526 (2005).

[41] K. B. Cooper, M. Steffen, R. McDermott, R. W. Simmonds, S. Oh, D. A. Hite, D. P. Pappas, and J. M. Martinis, Observation of Quantum Oscillations between a Josephson Phase Qubit and a Microscopic Resonator Using Fast Readout, Physical Review Letters 93, 180401 (2004).

[42] R. W. Simmonds, K. M. Lang, D. A. Hite, S. Nam, D. P. Pappas, and J. M. Martinis, Decoherence in Josephson Phase Qubits from Junction Resonators, Physical Review Letters 93, 077003 (2004).

[43] Y. Yu, S.-L. Zhu, G. Sun, X. Wen, N. Dong, J. Chen, P. Wu, and S. Han, Quantum Jumps between Macroscopic Quantum States of a Superconducting Qubit Coupled to a Microscopic Two-Level System, Physical Review Letters 101, 157001 (2008).

[44] J. M. Martinis, M. H. Devoret, and J. Clarke, Experimental tests for the quantum behavior of a macroscopic degree of freedom: The phase difference across a Josephson junction, Physical Review B 35, 4682 (1987).

[45] S.-X. Li, Y. Yu, Y. Zhang, W. Qiu, S. Han, and Z. Wang, Quantitative study of macroscopic quantum tunneling in a dc SQUID: A system with two degrees of freedom, Physical review letters 89, 098301 (2002).

[46] S.-X. Li, W. Qiu, S. Han, Y. Wei, X. Zhu, C. Gu, S. Zhao, and H. Wang, Observation of macroscopic quantum tunneling in a single Bi 2 Sr 2 CaCu 2 O 8+ δ surface intrinsic Josephson junction, Physical review letters 99, 037002 (2007).

[47] Y. Tian, H. Yu, H. Deng, G. Xue, D. Liu, Y. Ren, G. Chen, D. Zheng, X. Jing, and L. Lu, A cryogen-free dilution refrigerator based Josephson qubit measurement system, Review of Scientific Instruments 83, 033907 (2012).

[48] R. Rouse, S. Han, and J. Lukens, Observation of resonant tunneling between macroscopically distinct quantum levels, Physical review letters 75, 1614 (1995).
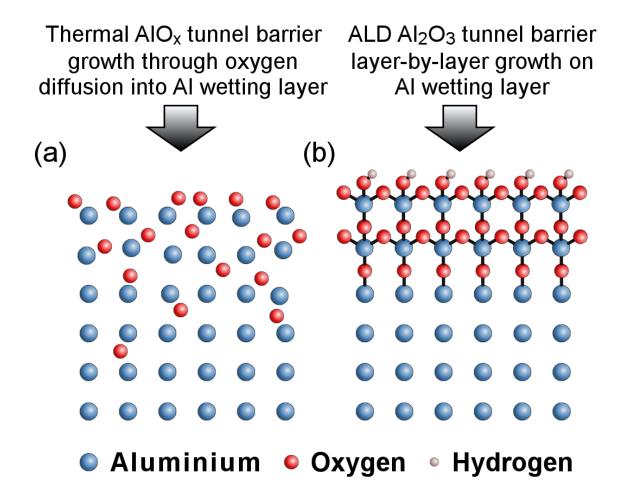
FIG. 1. Illustration which shows the structural differences between the (a) thermal AlO_x tunnel barrier, formed through oxygen diffusion into the Al wetting layer, and (b) the ALD Al_2O_3 tunnel barrier, formed through layer-by-layer atomic layer deposition of Al_2O_3.
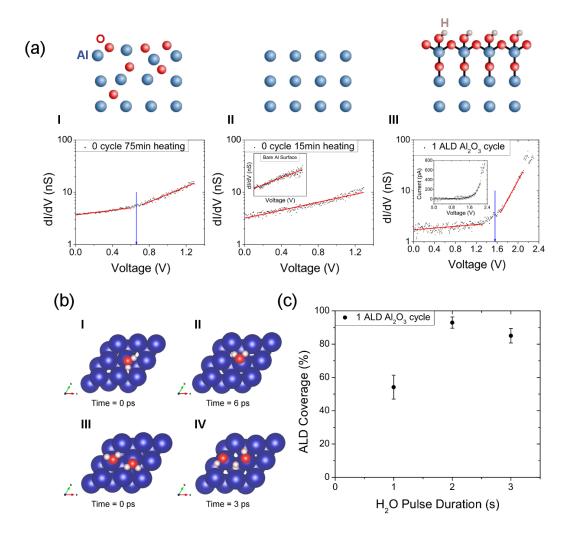
FIG. 2.   AIMD simulation and STS study of the ALD Al_2O_3 growth on an Al wetting layer from the pre-ALD sample heating to the 1st ALD Al_2O_3 cycle (0.12 nm/cycle). (a) Exemplary STS *dI/dV* spectra are plotted for an Al sample after (I) 75 min heating in the ALD chamber, (II) after 15 min of heating, and (III) after one ALD Al_2O_3 cycle. The arrows (blue) depict the tunnel barrier height, calculated as the intersection of the fit lines (red). Diagrams (top) illustrate the expected surface as seen by the STM tip. The insert in (II) is the *dI/dV* spectrum of a sample that was directly transferred to the STM chamber after Al sputtering and the insert in (III) is the corresponding IV curve for the 1-cycle ALD Al_2O_3 *dI/dV* spectra. (b) AIMD simulations are shown for H_2O adsorption onto an Al (111) surface. When only one H_2O molecule is present on the Al surface, dissociation is thermodynamically unfavorable (I, II). However, when H_2O

molecules are in close proximity, dissociation into OH⁻ and H⁺ is nearly instantaneous (III, IV). (c) The percentage of the Al surface which had a barrier height consistent with ALD Al_2O_3 after one ALD Al_2O_3 cycle with a variable initial H_2O pulse duration.
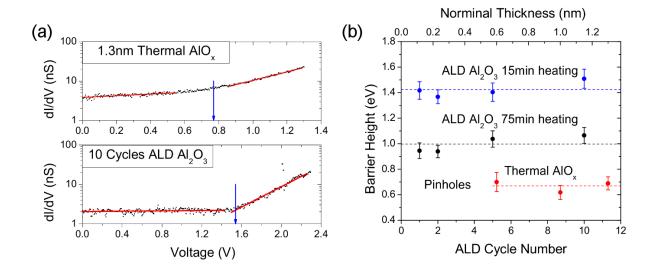

FIG. 3. A comparative STS study of ALD Al_2O_3 vs. thermal AlO_x tunnel barriers. (a) Exemplary constant height *dI/dV* spectra were taken on a 1.3 nm thermal AlO_x tunnel barrier (top) and a 10 cycle (1.2 nm) ALD Al_2O_3 tunnel barrier (bottom) with 15 min heating. The arrows (blue) depict the tunnel barrier height calculated as the intersection of the fit lines (red). (b) The average tunnel barrier height (dashed lines) for thermal AlO_x (red) and the ALD Al_2O_3 (blue-15 min and black-75 min heating,) tunnel barriers plotted as function of tunnel barrier thickness respectively.
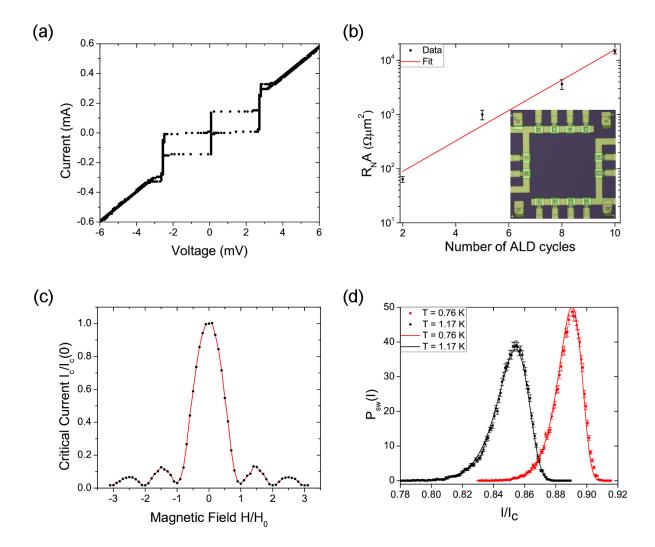
FIG. 4.   Nb/Al/Al$_2$O$_3$/Nb Josephson Junctions with an ALD Al$_2$O$_3$ tunnel barrier were measured. (a) The I-V characteristics of a 5 ALD cycle 10 μm x 10 μm Josephson Junction at T = 4.2 K is shown which displays a very low leakage current. The bias current waveform was triangular at 5 Hz and was ramped up linearly from zero to 0.6 mA, then from 0.6 mA to -0.6 mA, and finally from -0.6 mA to zero. (b) The critical current density, J_c, as a function of ALD cycle, or equivalently thickness, which follows the expected exponential dependence (solid line). The insert shows a chip with 12 JJs with areas ranging from 5 μm x 5 μm to 10 μm x 10 μm (c) The magnetic field dependence of the average switching current is shown for a similar 5-cycle JJ processed from the same batch. The Magnetic field and switching current have been normalized to the field at the 1st minimum (12 Oe) and the switching current at the central maximum (76

μA). (d) The measured switching current distributions of a 10-cycle junction at $T = 0.76$ K and 1.17 K. The lines are calculated switching current distributions based on thermal activation theory.